DOI 10.4430/bgta0359

The impact of multiple transmitters on signal strength in Deep Electrical Resistivity Tomography data: an experiment in the Vajont valley (north-eastern Italy)

F. Bocchia[1], R.G. Francese[1, 2], M. Giorgi[2], F. Fischanger[3] and S. Picotti[2]

[1] *University of Parma, Department of Chemistry, Life and Environmental Sustainability Sciences (S.C.V.S.A.), Parma, Italy*
[2] *National Institute of Oceanography and Experimental Geophysics (OGS), Trieste, Italy*
[3] *Geostudi Astier, Livorno, Italy*

(Received: 26 October 2020; accepted: 25 March 2021; published online: 3 December 2021)

ABSTRACT Electrical Resistivity Tomography method has boosted its potentials since the development of new-concept resistivity-meters. Key improvements include a much better data quality and the reduced logistics required to operate long spreads in rough terrains. The Multi-Source (MS) resistivity-meter incorporates both these two features and, moreover, its peculiarity of transmitting and receiving with short isolated wires reduces inductive and capacitive coupling in cables and multiplexer. It is a modular system based on stand-alone units remotely controlled via radio signals. Modularity eases the use of the system but the real innovative and most important feature is its capability of injecting current simultaneously with different dipoles. The system was tested in the Vajont valley, in north-eastern Italy, with the purpose of imaging the deep sliding surface of the catastrophic landslide occurred in 1963. An array of potential loggers was laid down parallel to the MS line in order to gain full control on transmitted/received signal character and strength and finally validate the system reliability. The MS waveform was clearly recognisable up to a distance of more than 1 km in single transmitter mode, while using multiple transmitters the threshold distance is probably far beyond and it was not reached. A potential of 0.02 mV was identified as the detection threshold. A one-to-one correspondence was observed, also at maximum offset, between MS measurements and potential values recorded with the data loggers indicating the effectiveness of the tested system in removing self-potentials.

Key words: subsurface resistivity, Multi-Source, DERT Deep Electrical Resistivity Tomography, Vajont, transceivers.

1. Introduction

High-resolution resistivity imaging via electrical tomography is already an up-to-date method and almost a standard approach to address a variety of geophysical problems (Chambers *et al.*, 2011; Schmidt-Hatterberger *et al.*, 2016; Tejero-Andrade *et al.*, 2018; Carrier *et al.*, 2019; Hojat *et al.*, 2020). This technique, in three decades since its first applications, reached a mature stage and data acquisition, processing, and interpretation are fairly consolidated procedures (Perrone *et al.*, 2014). The use of high-power transmitters (Rizzo and Giampaolo, 2019; Troiano *et al.*, 2019) was

a further expansion of the Electrical Resistivity Tomography (ERT) delivering a larger depth of exploration so that the method is often indicated as Deep ERT (DERT).

In the last few years several manufactures attempted a radical innovation of the method itself and in this scenario the development of the Multi-Source (MS) Resistivity system was certainly a major breakthrough (LaBrecque *et al.*, 2013a). The new concepts behind the system are essentially the modularity and the plurality with respect to traditional ERT resistivity-meters. These key features allow for overcoming the typical limitations of field deployment in rough terrains and the low signal generally detectable at large depths.

The MS has already been utilised in a variety of geological settings but, unfortunately, very few papers have been published on this topic, resulting in limited knowledge on system potentials and associated results (LaBrecque *et al.*, 2013b). Some authors have already used the MS for geothermal reservoir imaging, glacier thickness mapping (Picotti *et al.*, 2017), landslide hazard assessment (Chelli *et al.*, 2020), hydrogeological purposes and also, very recently, for levee imaging (M. Giorgi, personal communication). A key issue that was not yet investigated in details, and that is addressed by this paper, is the degree of confidence on the measured values of the artificial potentials and the effectiveness in propagating the electrical field at large distances using single and multiple transmitters.

An experimental survey was, then, designed and conducted in the Vajont valley in northern Italy, right on the top of the 1963 landslide body. The study site was selected because of the availability of several geological constraints and based also on the *a-priori* knowledge of the resistivity response of the landslide materials and of the underlying bedrock. The area was studied with traditional resistivity techniques (Francese *et al.*, 2013; Böhm *et al.*, 2014) as well as with the MS (LaBrecque *et al.*, 2013b) and with the Full Wave system. The two last surveys were both successful in mapping the sliding surface that is located approximately 250 m below the surface.

The potentials were measured at increasing distances from the transmitters using the MS itself and at the same time the potentials were monitored with an array of data loggers (DLs) operating for several hours at the frequency of 100 Hz. The potential time series were, then, correlated with the current injection and the waveforms were analysed in terms of overall signal amplitude and of cumulative response of multiple transmitters.

2. General settings

The Vajont valley is located in north-eastern Alps in Italy (Fig. 1), at the border between Veneto and Friuli-Venezia Giulia regions. The area is known worldwide for the catastrophic rockslide (Ghirotti, 1994; Genevois and Ghirotti, 2005) occurred in 1963 that caused almost 2000 deaths (De Nardi, 1965; Kiersch, 1965). At the time, the northern slope of Mt. Toc collapsed in a hydroelectric reservoir causing a giant wave that overtopped the dam and wiped out several villages around the reservoir in the underneath Piave valley.

The geology of the area is comprised of terrains aging from Upper Triassic to Eocene (Fig. 1), corresponding to the escarpment succession between the Belluno basin, on the west, and the Friuli platform, on the east (Picotti and Cobianchi, 2017). The glided succession (aging from Upper Jurassic to Upper Cretaceous) is bounded, at the bottom, by the Vajont Limestone and, at the top, by the Scaglia Rossa Formation. The stratigraphic series is comprised of the following units:

1) Vajont Limestone (Middle Jurassic): massive to stratified brownish oolitic limestones, interbedded with thin levels of micrite and intra-formational breccia. The formation thickness is approximately 450 m;

2) Fonzaso Formation (Middle - Upper Jurassic): comprised of calcite sandstones and brownish micritic limestones. The overall thickness of the formation ranges between 10 and 40 m;

3) Rosso Ammonitico Formation (Upper Jurassic): nodular, greyish and massive micrites containing Ammonoides. It forms a condensed sequence of pelagic high exhibiting a maximum thickness of 15 m;

4) Soccher Limestone (Lower - Upper Cretaceous): succession of limestones, calcarenites and bioclastic-intraclastic calcirudites, belonging to the paleo-domain of the calcareous Friuli platform. These first are interbedded with greyish, reddish and greenish micritic marbles, containing the real marker of this unit, i.e. nodular or bedded flint showing the same colours of marble. The total thickness of the formation is approximately 150 m.

5) Scaglia Rossa Formation (Upper Cretaceous - Lower Paleocene): a 300 m sequence of marls and reddish, marly limestones.

The structural framework of the Vajont valley is rather complicated (Fig. 1). The most prominent features are represented by two consecutive folds: namely, the Erto syncline and the Pelf-Frugna anticline. The axis of the first one is oriented approximately NW-SE, and cuts throughout the mid portion of the Vajont valley. The Pelf-Frugna anticline axis is oriented SW-NE and moves from the nearby Gallina valley to the south edge of the Vajont valley. These structures indicate a strong compression along the N-S direction, but they also show an E-W oriented component, with the stratigraphic succession gently dipping (15-20°) to the east.

The Erto syncline, on the northern flank of the Vajont valley, is abruptly interrupted by two longitudinal (E-W oriented) structures: the Mt. Salta line and the Spesse line, i.e. two SW-verging thrusts. The major effect of these faults is the doubling of the stratigraphic sequence described before on the north side of the valley. Other important structures are present on the northern slope of Mt. Toc and they are represented by high-angle faults. The structures oriented E-W are the Col delle Erghene fault (CE in Fig. 1) and the Costa Vasei-Calta fault (CVC in Fig. 1) while some other structures are oriented N-S and they are: the Col delle Tosatte fault (CTo in Fig. 1), the Col Tramontin fault (CTr in Fig. 1) and the Croda Bianca fault (CB in Fig. 1).

The orientation of these features depends upon the Alpine orogeny. The study area is included in the geological domain of the Southern Alps (i.e. the retrobelt stretch of the Alpine chain). The primary features of the Southern Alps are a series of south-verging fold-and-thrust structures, developed since the late Cretaceous. Secondary and more recent features are west-verging and they are associated with the stress field of the nearby Dinaric chain. This field of forces acted on a paleogeography made of a typical basin - carbonate platform succession where the studied area was located along the western margin of the Friuli Carbonate platform right at the border with the Belluno basin.

3. Materials and methods

The geophysical properties of the local succession, in terms of elastic wave velocity (Garbin and Vanin, 1986; Böhm *et al.*, 2014) and electrical resistivity, are variable, due to the hard-soft rocks alternation (Francese *et al.*, 2013), especially in the Jurassic-Cretaceous portion. The measurements collected on the undisturbed series, right on the Casso wall, indicate a range of 0.5-1.1 kΩ·m for the upper portion of the Fonzaso Formation, while the Soccher Limestone

range from 2.5 to 4.5 kΩ·m. The investigated sequence ends up with the Scaglia Rossa Formation, which resistivity is 0.5-1.0 kΩ·m.

Resistivity data are not directly available for the Vajont Limestone but resistivity is expected to be higher than 10 kΩ·m. Some laboratory measurements conducted during dam construction on dry samples resulted in resistivity values of 15-18 kΩ·m (Fondazione Lerici, 1960).

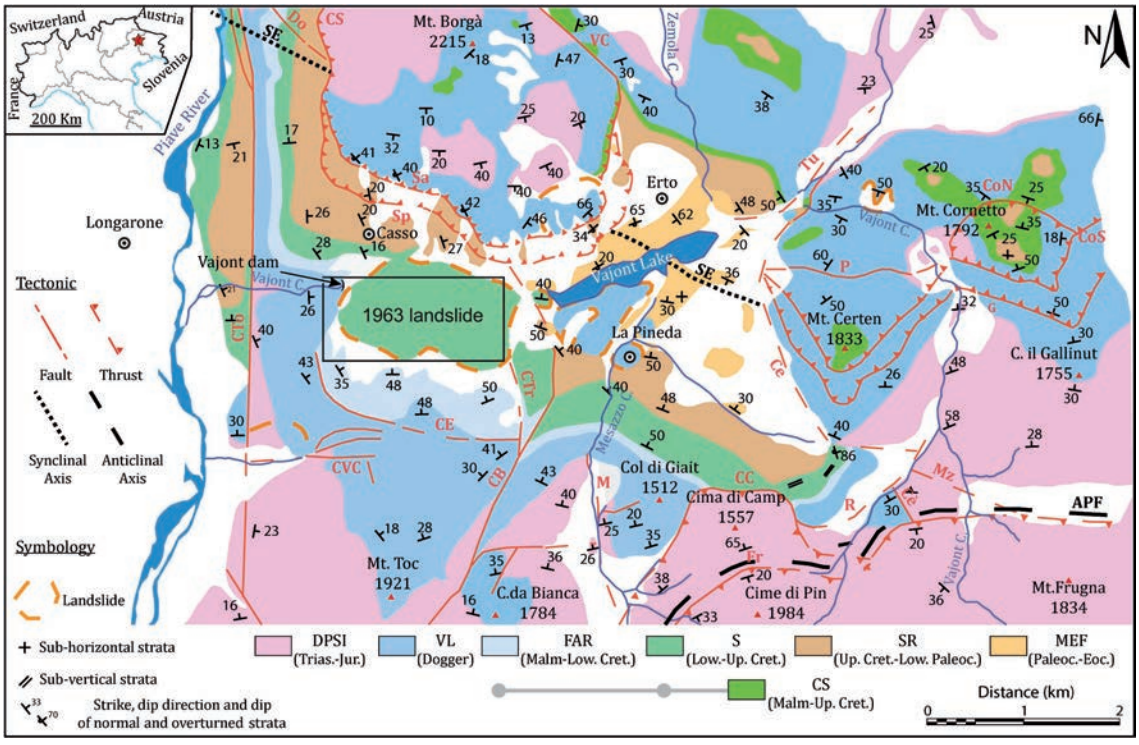

Fig. 1 - Geological setting of the Vajont area (modified from Riva *et al.*, 1990). DPSI: Dolomia Principale, Soverzene and Igne Fms; VL: Vajont Limestone; FAR: Fonzaso and Rosso Ammonitico Fms; S: Soccher Fm; SR: Scaglia Rossa Fm; MEF: Erto Marls and Flysch Fms; CS: Condensed Series; Do: "Dogarei" fault; CS: "Col Sparavièr" fault; VC: "Valon di Copàda" fault; Sa: "Monte Salta" fault; Sp: "Spesse" fault; Tu: "Val Tuora" fault; CTo: "Col delle Tosatte" fault; CoN: "Cornetto del Nord" fault; CoS: "Cornetto del Sud" fault; P: "Periàt" fault; G: "Gallinùt" fault; Ce: "Certen" fault; CE: "Col delle Erghene" fault; CTr: "Col Tramontin" fault; CVC: "Costa-Vasei-Calta" faults; CB: "Croda Bianca" fault; M: "Val Mesazzo" fault; CC: "Cima di Camp" fault; R: "Roppe" fault; Mz:" Mezùgn" fault; Fr: "Ferròn" fault; Cè: "South Certen" fault. Experiment area is marked by a rectangle.

3.1. The Multi-Source system

Resistivity data were collected with the MS system (Multi-Phase Technologies, USA: https://www.mpt.com) firstly introduced in 2013 (La Brecque *et al.*, 2013a). The system is comprised of standalone units (called transceivers: transmitter-receivers) capable of both injecting currents and measuring the artificial potentials.

Every single unit is designed with 3 sockets on the frontal panel allowing the connection of up to three electrodes (Ei). The electrodes are gathered in dipoles using all the available combinations. Two short dipoles (E1-E2 and E2-E3) and a long dipole (E1-E3) are capable of injecting current and measuring the potentials. A radio antenna enables the communication

with the other units and the command console. An internal Global Positioning System (GPS) and a 12 V (240 Wh) NiMH battery for power supply complete the transceiver box. The transmitter delivers a maximum power of 350 W resulting in a maximum voltage of 300 V and a maximum current of 2.5 A.

Each unit communicates directly with the command console and there is no need to deploy the transceivers at each other sight. Radio signal easily reaches transceivers located more than 2 km far apart. Morphology is not a major obstacle although in case of long deployments transceiver antennas could be lifted from ground level using portable mount poles.

The electrodes are wired to the unit but, since there is no physical connection between different units and between the units and the command console, this system can be considered wireless.

The system is operated by a field laptop connected to a mobile radio station. The units could be, then, remotely controlled up to distances of few kilometres.

The possibility of deploying the MS units without the constraints of a physical line connecting the 3-electrode gathers results in large degree of freedom in setting up the survey geometry especially in areas with rough terrains, rivers, roads or other infrastructures (LaBrecque *et al.*, 2013b). This is a major achievement in the MS design and the system itself represents the first available wireless resistivity-meter. The maximum number of units manageable by a single system counts up to 255.

The second, and probably the most innovative, feature of the MS is its capability of injecting current in the subsurface with multiple dipoles simultaneously. The goal is to increase the signal level with respect to existing systems. In a traditional approach, the power required to double the signal intensity is four times and reaching deep targets using standard 12V batteries without a power generator is not realistic. A possible alternative is to increase the signal intensity, for large-scale surveys, allowing multiple units to transmit in parallel (LaBrecque *et al.*, 2013b). In this configuration the standard 12V batteries are still usable. High-power transmitters, although very effective in increasing the depth of investigation, pose severe safety issues as well as many other logistical problems (mob/demob of a power generator, need of gasoline, noise concerns, etc.).

The major limitation in the MS system concept is that *n*-different transmitting-dipoles correspond to *n*-different transceiver units and that transmitting and receiving dipoles always correspond to different physical units.

The measurement in the MS system, similarly to other instruments, takes place in 4 steps (Fig. 2):

1) the electrical current is injected for a period (*Ttx*) of 1/(4·base frequency) (e.g. with a base frequency of 1 Hz the period of transmission is equal to 0.250 s);
2) the unit waits for a specific time interval (usually 0.010 s), namely the Resistivity Time Delay (TRDely), and, then, measures the voltage averaged on the Resistivity Measurement Time (TlnghtR, ~0.017 s);
3) the current is turned off for a period *Ttx*, meanwhile the TDIP decay waveform is measured during one or more windows;
4) the polarity is then inverted and the measures are repeated closing the cycle.

The default MS signal is composed by a 3-stack square wave, with each stack comprised of 2 cycles. The final waveform is then comprised of 3×2 = 6 cycles. IP measurements are taken in the same acquisition cycle.

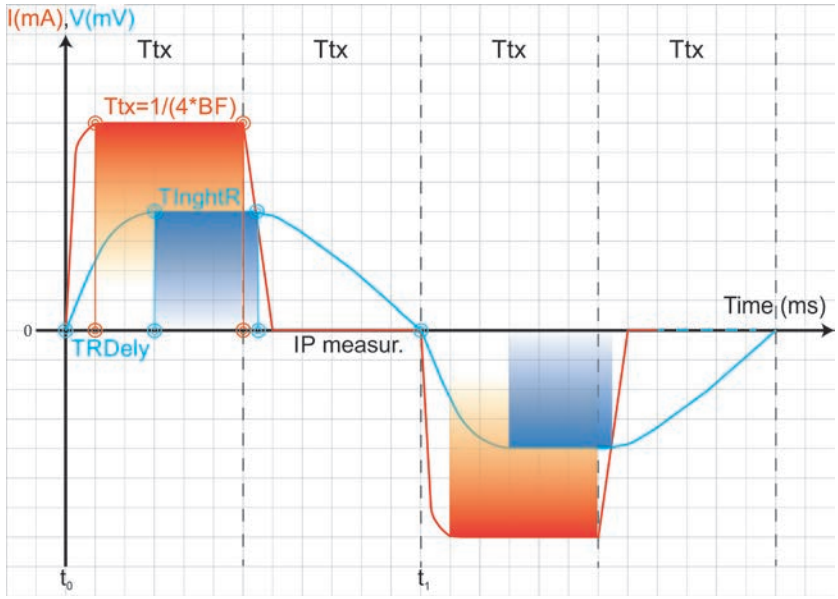

Fig. 2 - Sketch of the MS input waveform: BF stands for base frequency (generally 1 Hz); TRDely: Resistivity Time Delay; TlnghtR: Resistivity Measurement Time; IP measur.: represents the time span of IP measuring. The first cycle starts at $t_0 = 0$ ms and ends up at $t_1 = t_0 + dt$ ms. The horizontal axis is time in ms, while the vertical axis is current (A) in mA or voltage (V) in mV.

3.2. Experiment setup

The MS line was oriented more or less E-W and it extended from the southern shoulder of the Vajont gorge, nearby the dam, to the smaller lobe of the rockslide towards the locality La Pineda (Fig. 3). Eight transceiver units were available for the survey.

Transceivers were gathered in two blocks of 4 units each (b1, b2, b3, etc. in Table 1) and the electrode spacing was set to 25 m. Each block could operate both as transmitter (TX) or receiver (RX intra- and extra-block). The number of transmitting dipoles was doubled at each session until the maximum number of 4 was reached. In the 4TX configuration, a block operated as a unique transmitter, using at least an injecting dipole per transceiver, and the other block operated as a multi-dipole receiver. The rolling scheme (Table 1) was designed in order to cover the survey without exceeding the macro-distance factor *N* of five (e.g. b1-b5, b2-b6, b3-b7 in Table 1). The transmitting block was, then, moved forwards and the acquisition scheme was repeated until the receiving block was moved four stations apart. Reciprocal measurements (for 1TX only) have been also collected at each block station. A distance of 2.1 km was covered using 18 blocks (e.g. b1-b2, b1-b3, …, b2-b3, …, b6-b7) for a total of 28 transceiver stations resulting in 84 electrode positions along the survey line (Table 1).

Data, due to MS system design, could be collected in dipole-dipole mode only. Using this field configuration, the maximum aperture of the transmitting dipole was of 50 m (the external electrodes of each transceiver unit).

Continuous potential logging, using DLs, was carried out during several MS runs (Table 1). Among these, run R4 (blocks b1-b5) and run R5 (blocks b2-b3) were selected for signal analysis because of their larger offset with respect to DLs (Fig. 3).

During run R4 (blocks b1-b5) the current was injected right into the landslide body and in the

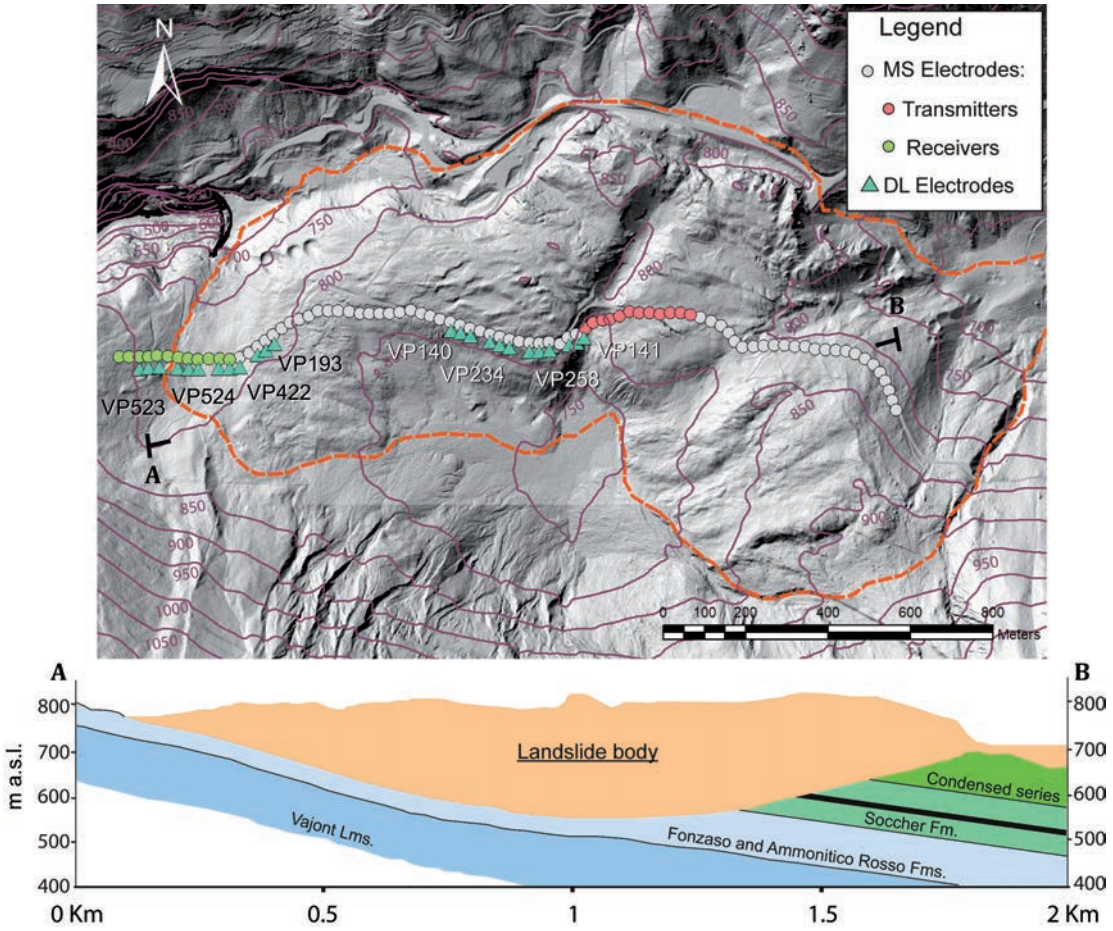

Fig. 3 - Data acquisition deployment (a); MS electrode positions are indicated with circles. Red and green circles indicate transmitters and receivers respectively (during a specific run of the experiment, see Table 1 for details). Schematic geological cross-section (b) below the survey line (modified from Broili, 1967). VL: Vajont Limestone; FAR: Fonzaso and Ammonitico Rosso Fms; S: Soccher Fm; SR: Scaglia Rossa Fm; MEF: Erto Marls and Flysch Fms; CS: Condensed Series.

Table 1 - MS data acquisition scheme. Potentials were logged in the first week of October, 2019; run R4 (blocks b1-b5) and run R5 (blocks b2-b3) were selected for signal analysis.

Run	TX-RX blocks	b1				b2				b3				b4				b5				b6				b7		
R1	b1-b2	1	2	3	4	5	6	7	8																			
R2	b1-b3	1	2	3	4					9	10	11	12															
R3	b1-b4	1	2	3	4									13	14	15	16											
R4	b1-b5	1	2	3	4													17	18	19	20							
R5	b2-b3					5	6	7	8	9	10	11	12															
R6	b2-b4					5	6	7	8					13	14	15	16											
R7	b2-b5					5	6	7	8									17	18	19	20							
R8	b2-b6					5	6	7	8													21	22	23	24			
R9	b3-b4									9	10	11	12	13	14	15	16											
R10	b3-b5									9	10	11	12					17	18	19	20							
R11	b3-b6									9	10	11	12									21	22	23	24			
R12	b3-b7									9	10	11	12													25	26	27
R13	b4-b5													13	14	15	16	17	18	19	20							
R14	b4-b6													13	14	15	16					21	22	23	24			
R15	b4-b7													13	14	15	16									25	26	27
R16	b5-b6																	17	18	19	20	21	22	23	24			
R17	b5-b7																	17	18	19	20					25	26	27
R18	b6-b7																					21	22	23	24	25	26	27

bedrock and the potentials were similarly measured on the bedrock and on the landslide body itself (Fig. 3). The injections of block b1 were not taken into considerations because too close to the DLs. In run R5 (blocks b2-b3) transmitters and receivers were both located on the landslide body. Results from run R4 are discussed in this paper.

4. Forward modelling

During survey planning, expected voltage (V) along the survey line were modelled with the ERT_Design modelling package (https://www.fischanger.it/ertdesign_ms/docs/EN/index.html).

Required input parameters are the line geometry as well as the intensity of the injected current and the background resistivity. Current intensity was established based on a 2013 MS experiment while background resistivity was averaged from previous traditional surveys (Francese *et al.*, 2013; Böhm *et al.*, 2014) but also considering the 2013 MS data. The MS can inject a maximum of 2500 mA at low contact resistances and imposes a maximum of 300 V on higher contact resistances. The expected contact resistances at the Vajont site are around 0.5-0.6 kΩ and the MS could push up to 500 mA of current.

A current of 500 mA along with a background resistivity 1.3 kΩ·m were then used in the simulations. Particular attention was devoted to the analysis of the Depth Of Investigation [DOI, *sensu* Oldenburg and Li (1999)] and to the amplitude of the artificial potentials measured at each transceiver unit.

The MS system is designed to work only in a dipole-dipole configuration, thus the DOI is related to the Normalised Depth of Investigation Characteristic (NDIC) equation (Edwards, 1977; Barker, 1989):

$$NDIC = n(n+1)(n+2)\left(\frac{2zdz}{a^2}\right)\left\{\left[n^2+4\left(\frac{z}{a}\right)^2\right]^{-3/2} - 2\left[(n+1)^2+4\left(\frac{z}{a}\right)^2\right]^{-\frac{3}{2}} + \left[(n+2)^2+4\left(\frac{z}{a}\right)^2\right]^{-3/2}\right\}. \quad (1)$$

In Eq. 1, a is the dipole length, n is the order of the measure or the separation between dipoles expressed as a multiple of dipole lengths, and z is the depth.

The DOI is estimated, first, integrating the analytic sensitivity function, for the given n-pole, and after by calculating the median z depth, so that the area under the sensitivity curve is equal to the 50% of the total area (Edwards, 1977).

All the transmitters were assigned to block b5 (Table 1) using transceiver units from 17 to 20.

4.1. Simulation 1TX - Single-transmitter mode

With a single transmitting dipole (unit 20 electrodes P2 and P3) (Fig. 4a) the expected V reaches a maximum of about 1000 mV nearby current injection (exceeding the value of 1000 mV at the closest electrodes of unit 21). Minimal V values are observed at the far receivers and several dipoles show signals below the critical modelling threshold of 0.1 mV (the potential drops down to 0.035 mV at electrodes P1-P2 of unit 1). The general trend of the DOI curve is somewhat opposite since an increasing separation between transmitting and receiving dipoles corresponds to a greater depth of investigation. Using a single transmitter the farthermost reliable measure occurs at electrodes 1-2 (P2-P1 in Fig. 4a) of unit 5. The DOI for this dipole is ~270 m while its maximum sensitivity is reached at approximately 200 m of depth.

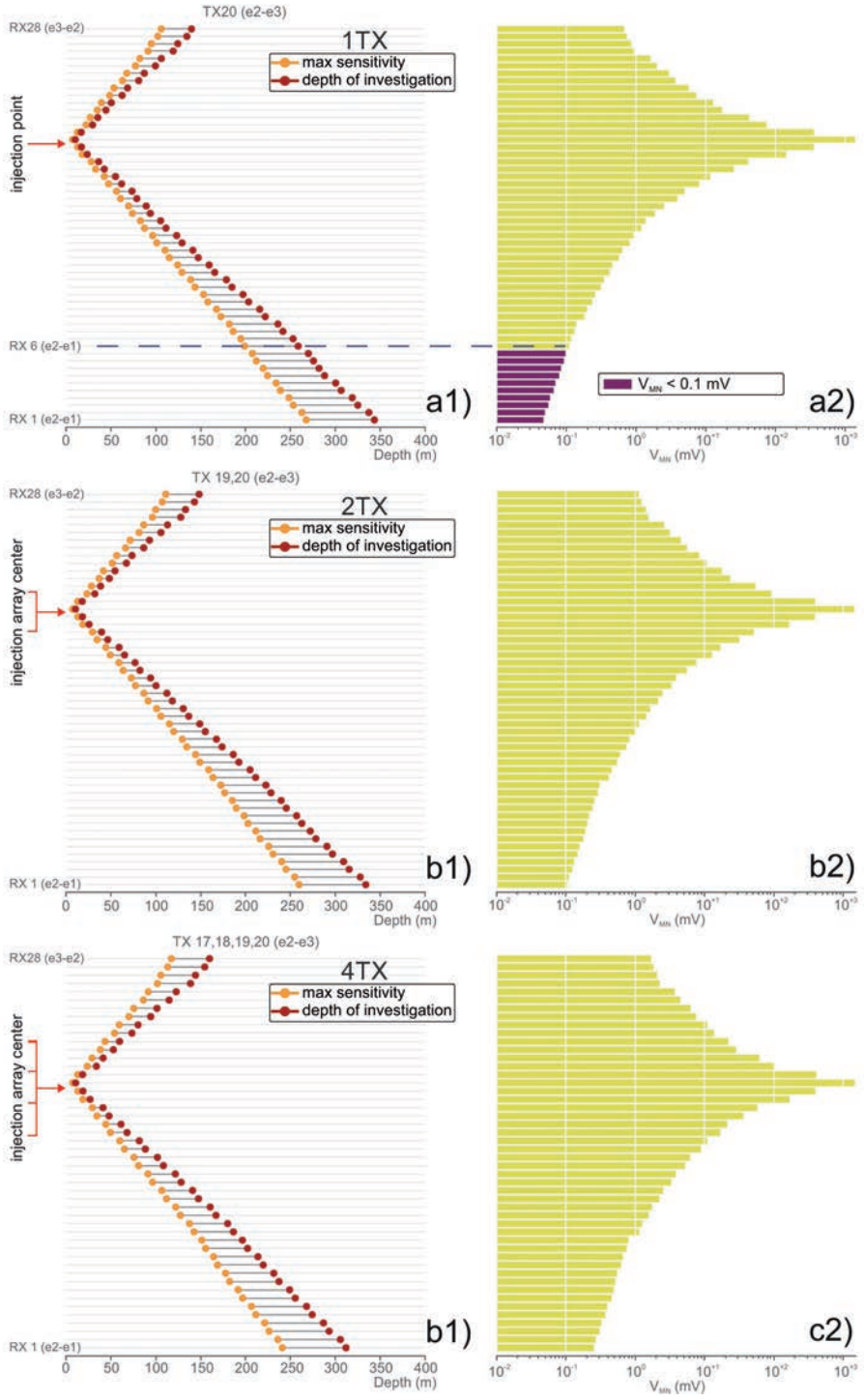

Fig. 4 - Results of numerical simulations: 1TX, single-transmitter (a); 2TX, multiple-transmitters (b); 4TX, multiple transmitters (c). Depth of investigation and maximum sensitivity for each receiving dipole (transmission occurring in block b5) are visible on the left panels (a1, b1, and c1); expected potentials at each receiving dipole, with a stable current intensity of 500 mA and a background resistivity of 1300 Ω·m, are visible on the right panels (a2, b2, and c2). All transceiver stations (RX1, RX2, …, RX28) with two couples of electrode each (e2-e1 and e3-e2) have been considered for simulation.

4.2. Simulation 2TX - Multiple-transmitter mode

With an additional transmitter (two transmitting dipoles: unit 19 and unit 20, electrodes P2 and P3) the expected V remains more or less similar nearby the current injection point while it increases significantly at the outer receiving dipoles (Fig. 4b). The expected V of the totality of the dipoles is beyond the critical modelling threshold of 0.1 mV. The DOI-Sensitivity graph is more or less similar to the single-transmitter case with a reduction of 3% in the overall values. This marginal reduction is mostly related to the slight reduction of the distance factor *N*.

4.3. Simulation 4TX - Multiple-transmitter mode

A major increase in the expected V signal could be observed adding two more transmitting dipoles (four transmitting dipoles: units 17, 18, 19, and 20, electrodes P2 and P3). Again, this is particularly evident at the far ends of the survey line, where the minimal potential values raised up to approximately 0.25 mV at unit 1 (Fig. 4c). The potentials in units from 8 to 28 are all above 1 mV while they are beyond 10 mV in the subset of units from 13 to 24. DOI and maximum sensitivity are now both affected by a visible reduction in their values because of the repositioning of TX and RX dipole centres that affected the distance factor *N*. The reduction is about 10% with respect to the single-transmitter configuration.

5. Results

In this section the results obtained are commented while monitoring the potentials during run R4 (blocks b1-b5).

5.1. Potentials measured by the MS system

The MS data set resulted of 11210 data points and more specifically of 5320 1TX values, 3990 2TX values, and 1900 4TX values.

A preliminary consideration could be done just by plotting recorded potentials vs. the geometric factor (*K*) for each quadrupole of the MS data set (Fig. 5). The geometric factor of the multi-transmitter was calculated considering the mid-point of the transmitting array. The measured potentials range from 0.01 to 10,000 mV while the geometric factor spans an interval of $1 \cdot 10^7$ units.

5.1.1. Data set 1TX - Single-transmitter mode

The plotted data points show a good fit with a power model and the coefficient of determination (R-squared) is 0.94. Potential values range from 0.01 to 1,000 mV with an average value of 107 mV.

5.1.2. Data set 2TX - Multiple-transmitters mode

The plotted data points show a much higher dispersion and the fit with a power model is not as good as in the previous case as the coefficient of determination (R-squared) lowers to 0.79. Potential values as expected increase and range from 0.01 to 2,900 mV with an average value of 119 mV.

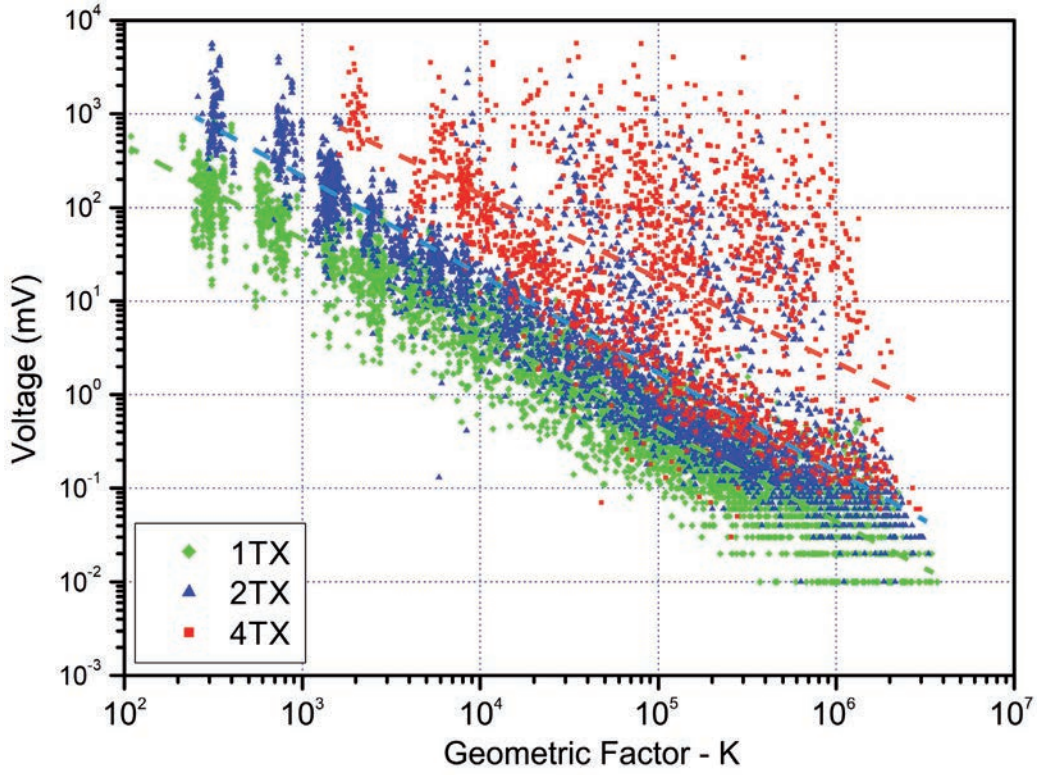

Fig. 5 - Measured voltage (V) plotted versus geometric factor (*K*): green dots represent V values recorded in single-transmitter mode (1TX), while blue and red dots stand for multiple-transmitter mode (2TX and 4TX) acquisitions.

5.1.3. Data set 4TX - Multiple-transmitter mode

The plotted data points appear to be rather dispersed and the fit with a power model is poor showing a coefficient of determination (R-squared) of 0.33. Potential values range from 0.03 to 5,700 mV with an average value of 176 mV.

5.2. Potentials measured with the DLs

A total of 8 DLs recorded the potentials during run R4 (b1-b5). The current injection occurred at block b5 and the distance between each DL and the centroid of the transmitting array ranges from 470 to 1350 m. Data from logger VP258 are just partly available because of poor electrode coupling during the first hour of the experiment.

Synchronisation between DLs and MS records was feasible because both the two systems incorporate a GPS clock for timing. In both the two data sets the UTC time stamp is recorded. The starting second, computed from midnight, is recorded in the MS data file for each current injection (single or multiple). The injection occurs at an exact second based on the Pulse Per Second (PPS) digital output available in the modern GPS modules. PPS is an output signal, which changes its value exactly on the 1 s. Once the starting second of the current injection was defined, a MATLAB routine, coded for this purpose, extracted the entire injection time window (6 s) from the potential time series of the DLs.

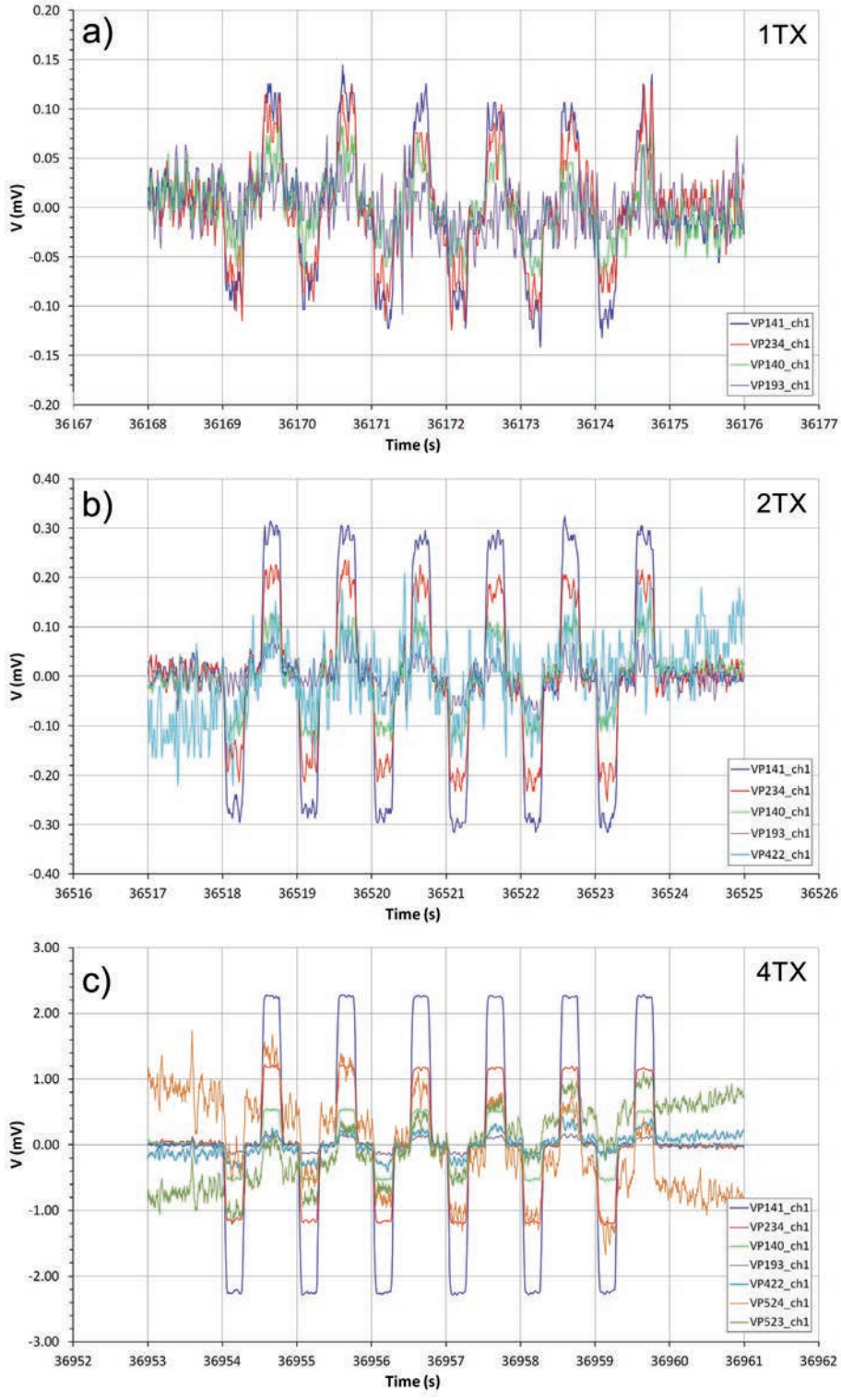

Fig. 6 - 6-peak wavelet recorded with the DLs in single- and multiple-transmitter mode at various distances; 1TX, single-transmitter (a): units VP141, VP234, VP140, and VP193; 2TX multiple-transmitters (b): units VP141, VP234, VP140, VP193, and VP422; 4TX, multiple transmitters (c): all the deployed units but VP254 that was malfunctioning; see text for explanation.

5.2.1. Data set 1TX - Single transmitter

The 6-cycle squared waveform is clearly visible (Fig. 6a) in the nearest logging units (VP141, VP234, VP140, and VP193) while in these Time Domain (TD) graphs is not really detectable in the outer logging units (VP422, VP524, and VP523). Potential values decay from 0.12-0.15 mV at inner unit VP141 to below 0.05 mV at outer unit VP193 where the current waveform is very noisy and barely visible.

5.2.2. Data set 2TX - Multiple transmitters

The 6-cycle squared waveform is visible (Fig. 6b) in the logging units VP141, VP234, VP140, VP193, and VP422 while in TD is still not detectable in the far logging units (VP524 and VP523). The waveform at unit VP193 appears now sharp and defined. Potential values decay from 0.30 mV at the closest unit VP151 to around 0.05 mV at the outer unit VP422 where the current waveform, although noisy, is clearly visible. The potentials recorded at unit VP422 show a positively biased trend.

5.2.3. Data set 4TX - Multiple transmitters

The 6-cycle squared waveform is visible (Fig. 6c) in the total of the deployed logging units. Potential values decay from 2.20 mV at the closest unit VP151 to around 0.75-0.80 mV at the far off unit VP523. Units VP524 and VP523 show in the potential curves positively and negatively biased trends, respectively.

6. Discussion

The detailed analysis of the potentials recorded from both the MS system itself and the DLs provided a series of key indications about the performance of this new-concept instrument.

The MS, due to design constraints, operates in dipole-dipole configuration only and this configuration is known to be quite noisy. In dipole-dipole mode the signal strength decays with inverse proportionality to the cube of the distance factor N (Loke, 2020). The N factor of 6 is prudentially considered a limit as the signal drops by about 56 times shifting from $N = 1$ to $N = 6$ (Loke, 2020). In the analysed data set, in single-transmitter mode (Fig. 7a), the ratio between the average of the potentials measured at $N = 1$ is equal to 55 times the average of the potentials measured at $N = 6$, in good agreement with Loke (2010) indications. Anyhow, it is worthwhile to notice how the measured potentials show a nice and sharp decreasing trend without the typical dispersion occurring in noisy data sets. The signal strength lowers below 1 mV starting from $N = 10$ and just for a minimum number of data points. The curve describing the average voltage per each distance factor remains almost always above the 1 mV value.

The recorded signals at $N > 10$ (i.e. with ratio higher than 300 times compared to measurements collected at $N = 1$) appear to be still valid as it will be showed later in this section.

The signal strength in multiple-transmitter mode increases significantly (Fig. 7b). The ratio 2TX/1TX, for $N = 10$ is equal to 2 while the ratio 4TX/1TX has a value larger than 10. These indications are just partly quantitative as there is not a consolidated way to calculate the distance factor N when using multiple transmitters. For the purpose of comparing the potentials, the distance factor for multiple transmitters was calculated averaging the maximum and minimum values.

In multiple-transmitter mode, the particular transmitting-receiving geometry experimented during the survey resulted particularly effective in stacking the electrical fields generated by the single transmitting dipole resulting in a better increase of the signal strength. The gathering of the available transceivers in two blocks comprised of four units each (in a sort of "super-transmitter" mode) significantly improved the signal intensity compared to previous MS surveys conducted with the fairly consolidated roll-along scheme.

The modelled potentials, although slightly higher compared to the real potentials measured by the MS during the survey, somewhat follow a theoretical behaviour (La Brecque *et al.*, 2013b).

The signal strength increases of 2.2 times doubling the transmitters from 1TX to 2TX in the farthermost units (dipole distance > 800 m) while in the inner units (dipole distance < 300 m) the expected signal strength, in 2TX mode, is more than 3 times the signal expected in 1TX mode (Fig. 7c).

The signal strength, further doubling the transmitters from 2TX to 4TX, increases of 5.5 times in the farthermost units (dipole distance > 800 m) while in the inner units (dipole distance < 300

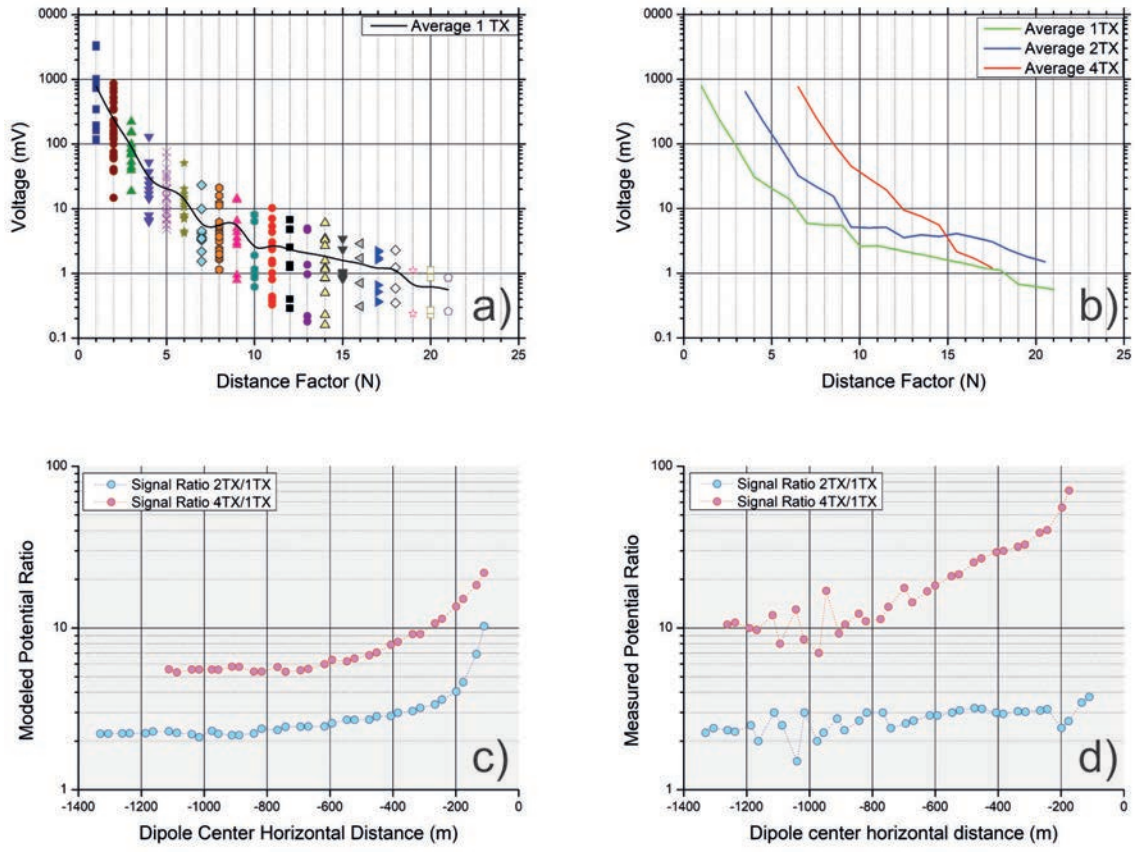

Fig. 7 - Potentials recorded in single-transmitter mode (a) plotted versus distance factor *N*. Curves describing the average of the potentials in 1TX, 2TX, and 4TX mode (b) plotted versus distance factor *N*. Potential ratio at increasing distance from the transmitter: signal ratio of the modeled potentials (c) switching from single-transmitter (1TX) to multiple-transmitter mode (two transmitters: 2TX) and from single-transmitter (1TX) to multiple-transmitter mode (four transmitters: 4TX). Same as above but with measured potentials (d). Transceivers are located westwards of transmitting block b5.

m) the expected signal strength, in 4TX mode, is more than 10 times the signal expected in 1TX mode (Fig. 7c).

The amplitude ratios of the real signals from single- to multiple-transmitters show comparable trends with the modelled signals. The signal strength increases about 2.4 times doubling the transmitters from 1TX to 2TX in the farthermost units (dipole distance > 800 m) while in the inner units (dipole distance < 300 m) the measured signal strength, in 2TX mode, is around 3 times the signal measured in 1TX mode (Fig. 7d). The signal ratio, further doubling the transmitters from 2TX to 4TX, increases up to 10 times in the farthermost units (dipole distance > 800 m) while it grows up quickly, similarly to modelled data, in the inner units. The apparent scattering of the ratios visible in the distance interval comprised between 800 and 1200 m is probably related to geological reasons. The landslide edge is located right at the fifth dipole midpoint. In this point there is a sudden jump between the outcropping bedrock and the landslide body (Fig. 3) and, moreover, this contact is probably occurring along a vertical fault. The electrical field is, then, distorted both by topographical gradients and by sudden lateral and vertical changes in subsurface resistivity.

DOI and maximum sensitivity are just marginally affected by the use of multiple transmitters. The reduction in the DOI, that in the worst case reaches the value of 10% (switching from single-transmitter to four-transmitter mode), could be easily compensated moving forwards the transmitting block and collecting just 2TX and 4TX data.

The difference between modelled and real data are mostly related to geological reasons and to the reduced current intensity injected in the real measurements. In the modelled potentials the injected current was set to 500 mA per each injecting dipole. The average intensity of the injected current was 200 mA in 1TX mode, 165 + 180 mA in 2TX mode and finally 180 + 190 + 205 + 175 mA in 4TX. These current intensities are 50-60% lower compared to the modelling parameters. Subsurface geology at the Vajont site is highly variable and the current measured in previous surveys was mostly devised by data collected using traditional resistivity-meters at different spots of the landslide hence, probably, the difference between the expected and

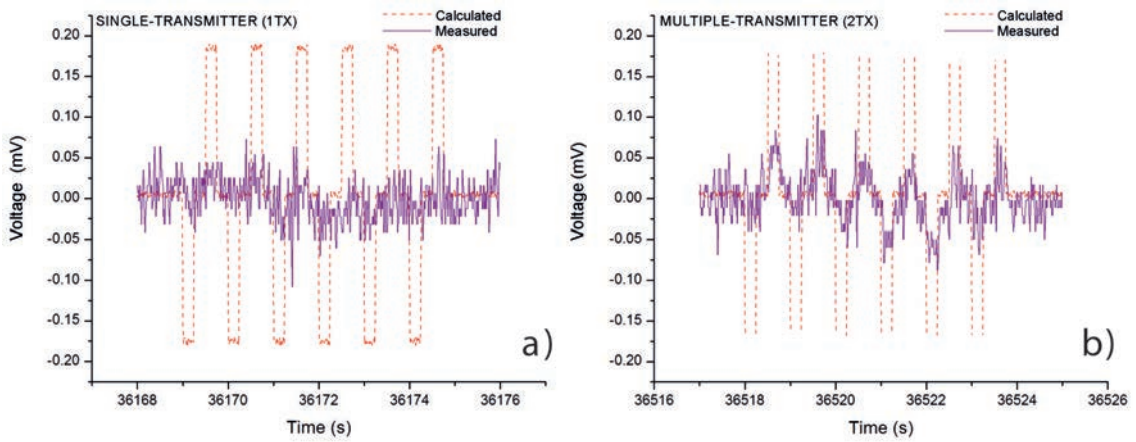

Fig. 8 - Potential measured at unit VP141; 1TX, single-transmitter (a): the receiving dipole is located at a distance of about 1150 m from the transmitting dipole; 2TX multiple-transmitters (b): the receiving dipole is located at a distance of about 1100 m from the transmitting array.

the real current intensity is strictly geology-dependent. Better convergence could be probably achieved lowering the modelled current intensity to 250 mA, but this was outside the target of the experiment.

Detailed analysis of the signal decay as moving apart from current injection dipole/s was the core of the experiment. Potential decay analysis for single and multiple transmitters was entirely conducted in TD visually matching the 6-cycle current injection with the recorded waveforms. In single-transmitter mode, the decay in space was quite rapid and at unit VP193, located at a distance of about 1150 m from the transmitter, the signal is barely recognisable but with a large degree of uncertainty (Fig. 8a). In multiple-transmitter mode (2TX), the signal is clearly recognisable at unit VP193 (Fig. 8b) and also far apart down to unit VP422, located at a distance of about 1200 m from the centre of the transmitting array (Fig. 6b).

Finally, in multiple-transmitter mode (4TX) the signal is clearly recognisable in all the deployed DLs to a maximum distance of 1270 m corresponding to the midpoint of the outer receiving dipole wired to unit VP523. The signal strength at unit VP524 and VP523 (Fig. 6c), although noise biased and affected by a clear self-potential trend, is 5 times higher than the signal measured at unit VP422 and VP193 that are much closer to the transmitting array. The jump of the potential occurs in less than 200 m and the reason is probably related to geology as VP524 and VP523 are located on the southern shoulder of the Vajont gorge right on the outcropping bedrock and the latter carries higher amplitude electrical signals. A possible cause of the evident trends visible on the potential curves is the presence of a nearby overhead power line with the supporting towers founded directly on the outcropping bedrock of the gorge shoulder.

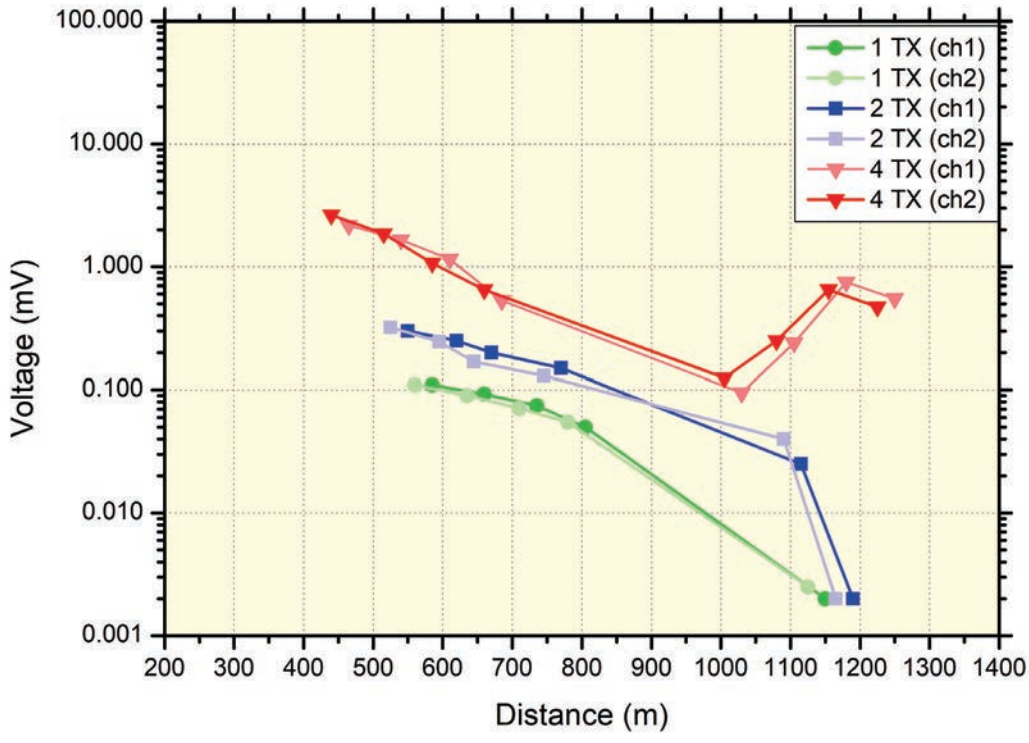

Fig. 9 - Plot of the voltage of the potential DLs versus transmitting-receiving distance for run R4 (blocks b2-b5); full and light colours indicate channel #1 (ch1) and channel #2 (ch2) of each DL.

The comprehensive plot of potential signals clearly shows the decay trend (Fig. 9). Channel #1 and channel #2 have been both plotted in the graph. The readings of 0.002 mV in single-transmitter mode (1TX) and in multiple-transmitter mode (2TX) are just guesses as the time series were barely interpretable so these data points should not be considered. The value of 0.025 and 0.040 mV in multiple-transmitter mode (2TX) should be considered reliable as the waveform was clearly recognisable in the time series.

The positive jump of the potentials in multiple-transmitter mode (4TX), occurring from the distance of 1000 m, has already been discussed and depends on geology.

The potential of 0.02 mV was identified as a primary threshold for the MS signals based on the visual analysis of the totality of the time series recorded with the DLs. Potentials with signal strength lower than this value have been never undoubtedly identified in the data. This threshold could be used as a limit for filtering the MS data before carrying out the inversion. In this experiment the analysis was conducted entirely in TD but it is possible that the threshold could be further lowered filtering out the short-period noise in Frequency Domain (FD). The value of 0.02 mV is much lower as compared to the value of 0.1 mV that among field geophysicists could be considered as a realistic lower limit in various scenarios of electrical noise.

The potential threshold could be also directly correlated with the concept of critical distance or maximum distance to take into consideration when collecting data with the MS system using single- and multiple-transmitters. This parameter could be very useful to design the survey and avoid collecting very noisy and poorly usable data. This was a major concern for surveying with the MS system as the signal strength due to the mandatory dipole-dipole acquisition geometry is always low in single-transmitter (1TX) mode.

The polynomial trend line function (with a coefficient of determination of 0.99) of the single-transmitter mode (1TX) intersects the threshold line at approximately 900 m while the last data point of the multiple-transmitter mode (2TX) is virtually on the threshold line at 1100 m.

The maximum distance for the single-transmitter (1TX) mode could be estimated in 0.9 km while it rises up to 1.1 km doubling the transmitters (2TX). Further doubling the transmitters (4TX) the critical distance was not really reached. The outcropping bedrock probably carries larger amplitude signals partly biasing the results.

To better understand the real potentials of transmitting with four dipoles (4TX) the MS and the DLs should be entirely deployed on the landslide body avoiding locating transmitters or receivers on the outcropping bedrock. Unfortunately, it is not as easy as geology on the eastern side the landslide is fairly more complicated with the superposition of a secondary collapsed lobe.

The above considerations on the signal threshold and on the determination of the maximum distance are valid for the Vajont site but they could be generalised to cases with similar background resistivity (i.e. 0.8-1.4 kΩ·m).

The very last issue to comment is the direct comparison between the potentials stored in the MS data set and the potentials extracted from the DLs. In the near to medium range (< 1000 m) there was no difference as the values were almost identical (less than 1% of difference) also at very low signal levels, thus validating the MS system.

The difference in the two farthermost DLs (VP524 and VP523) was much higher and ranging between 15% and 20%. These two DLs, as above discussed, were located on the outcropping calcareous rocks of the Vajont gorge at a distance of less than 100 m from an overhead power line. Self-potentials because of electrical and electro-magnetic noise are, then, rapidly changing, thus affecting the reading of the MS system.

6. Conclusions

The recently developed MS system, a novel-concept resistivity-meter, showed interesting application potentials and introduced a new approach for collecting DERT data.

The large array of DLs, deployed to cross-validate the MS resistivity-meter, recorded the potential signals at a sample rate of 10 ms and the resulting time series described, in details, the spatial and the temporal variation of both self- and source-generated potentials.

The time stamp, obtained via internal GPS PPS, was the key to correlate the two data sets. The *t*-uples stored for each MS transmission report the injection time synchronised at 1 s while the binary time series of the DLs are controlled by the GPS clock that sample the time signal every second. A series of MATLAB routine were coded to synchronise the two data sets and extract from the logged potential series a time window of 6 s for each current injection.

Potential decay analysis for single and multiple transmitters was entirely conducted in TD visually matching the 6-cycle current injection with the recorded waveforms. The potential of 0.02 mV was identified as a primary threshold for the MS signals. This value could be probably lowered with further and more advanced signal analysis to be carried out in FD. In FD part of the high-frequency noise could be filtered out but this was beyond the objectives of the experiment.

The critical distances, based on this threshold and on the electrical settings of the study site, could be estimated in 0.9 km for the 1TX configuration, in 1.1 km for the 2TX configuration, and beyond 1.3 km for the 4TX configuration. In the 4TX configuration, the critical distance could not be really reached but, for the sake of clarity, should be noticed that the asymmetry of the geology in the subsurface probably partly biased the results. The potentials recorded at the outmost logging units during run b1-b5 were located on the outcropping resistive bedrock that probably better carried the propagation of the artificial electrical field.

Modelled potentials are comparable in trend but not in the absolute values with the measured potentials. The misfit is ~20% for the 1TX data set, ~24% for the 2TX data set, and ~30% for the 4TX data set. The reason is partly due to the too high current intensity selected for the numerical simulations.

A final comment is dedicated to the sophisticated electronics of the MS system. We noticed almost a one-to-one correspondence between the potential values recorded in continuous with the DLs, averaged over 6 entire cycles, and the potential value stored in the MS data set. The capability of the MS system of effectively removing the self-potentials is really impressive, especially in the vicinity of the overhead power lines, where the self-potentials were changing at a very high rate.

The MS system could be, then, considered validated and the results of the detailed analysis conducted at the Vajont test site could be used as a benchmark for surveying in similar relatively resistive geological settings. More generally the results provide important indications for using the MS system to investigate deep geological targets.

Acknowledgements. Results from this experiment were presented during GNGTS meeting in Rome, 12-14 November 2019. Funding for the current project was provided by Regione Friuli Venezia Giulia, by the University of Parma (FILFrancese) and by the National Institute of Oceanography and Applied Geophysics - OGS. We gratefully thank Giancarlo Ceresoli from PROGEA Consulting S.r.l. for making the potential data loggers available and for the great aid during the field work and we also thank ADASTRA ENGINEERING S.r.l. for the assistance during land surveying.

REFERENCES

Barker R.D.; 1989: *Depth of investigation of collinear symmetrical four-electrode arrays*. Geophys., 54, 1031-1037.

Böhm G., Francese R. and Giorgi M.; 2014: *3D geophysical model of the Vajont rockslide from seismic and geoelectric surveys*. In: Proc. 20th European Meeting of Environmental and Engineering Geophysics, Near Surface eoscience 2014, Athens, Greece, Vol. 2014, pp. 1 - 5, doi: 10.3997/2214-4609.20142052.

Broili L.; 1967: *New knowledge on the geomorphology of the Vaiont slide slip surfaces*. Rock Mech. Eng. Geol., 5, 38-88.

Carrier A., Fischanger F., Gance J., Cocchiararo G., Morelli G. and Lupi M.; 2019: *Deep electrical resistivity tomography for the prospection of low- to medium-enthalpy geothermal resources*. Geophys. J. Int., 219, 2056-2072, doi: 10.1093/gji/ggz411.

Chambers J.E., Wilkinson P.B., Kuras O., Ford J.R., Gunn D.A., Meldrum P.I., Pennington C.V.L., Weller A.L., Hobbs P.R.N. and Ogilvy R.D.; 2011: *Three-dimensional geophysical anatomy of an active landslide in Lias Group mudrocks, Cleveland basin, UK*. Geomorphol., 125, 472-484, doi: 10.1016/j.geomorph.2010.09.017.

Chelli A., Francese R., Petrella R., Carri A., Quagliarini A., Segalini A., Caporicci M.P., Diena M., Giorgi M. and Celico F.; 2020: *A multi-parameter field monitoring system to investigate the dynamics of large earth slides-earth flows in the Northern Appennines, Italy*. Eng. Geol., 275, 105780, doi: 10.1016/j.enggeo.2020.105780.

De Nardi A.; 1965: *Il bacino del Vajont e la frana del M. Toc*. L'Universo, 45, 3-70.

Edward L.S.; 1977: *A modified pseudosection for resistivity and induced-polarization*. Geophys., 42, 1020-1036.

Fondazione Lerici; 1960: *Ricerche d'infiltrazione d'acqua nella roccia della diga del Vajont mediante misure elettriche in fori (prove sperimentali)*. Unpublished Technical Report.

Francese R., Giorgi M., Böhm G., Bistacchi A., Bondesan A., Massironi M. and Genevois R.; 2013: *3D geophysical imaging of the Vajont landslide and of its surroundings*. Ital. J. Eng. Geol. Environ., BS6, 555-565, doi: 10.4408/IJEGE.2013-06.B-53.

Garbin C. and Vanin V.; 1986: *Tunnel excavation in the Vajont slide*. In: Semenza E. and Melidoro G. (eds), Meeting on the 1963 Vaiont Landslide, International Association for Engineering Geology and the Environment - Italian Section, Ferrara, Italy, pp. 145-156.

Genevois R. and Ghirotti M.; 2005: *The 1963 Vaiont landslide*. Giornale di Geologia Applicata, 1, 41-52, doi: 10.1474/GGA.2005-01.0-05.0005.

Ghirotti M.; 1994: *Modellazione numerica della frana del Vajont sulla base di nuovi dati*. Geologica Romana, 30, 207-216.

Hojat A., Arosio D., Ivanov V.I., Loke M.H., Longoni L., Papini M., Tresoldi G. and Zanzi L.; 2020: *Quantifying seasonal 3d effects for permanent electrical resistivity tomography monitoring system along the embankment of an irrigation canal*. Near Surf. Geophys., 18, 427-443.

Kiersch G.A.; 1965: *Vaiont reservoir disaster*. Geotimes, May - June, pp. 9-12.

LaBrecque D., Casale D., Brigham R. and Flinchum B.; 2013a: *A multi-source approach for electrical resistivity tomography*. In: Symposium on the application of Geophysics to Engineering and Environmental Problems 2013, Environmental & Engineering Geophysical Society, p. 795, doi: 10.4133/sageep2013-230.1.

LaBrecque D.J., Morelli G., Fischanger F., Lamoureux P. and Brigham R.; 2013b: *Field trials of the multi-source approach for resistivity and induced polarization data acquisition*. In: Abstracts, AGU Fall Meeting, American Geophysical Union, San Francisco, CA, USA, NS34A-03.

Loke M.H.; 2020: *Tutorial: 2-D and 3-D electrical imaging surveys*.

Oldenburg D.W. and Li Y.; 1999: *Estimating depth of investigation in dc resistivity and IP surveys*. Geophys., 64, 403-416.

Perrone A., Lapenna V. and Piscitelli S.; 2014: *Electrical resistivity tomography technique for landslide investigation: a review*. Earth Sci. Rev., 135, 65-82, doi: 10.1016/j.earscirev.2014.04.002.

Picotti V. and Cobianchi M.; 2017: *Jurassic stratigraphy of the Belluno basin and Friuli platform: a perspective on far-field compression in the Adria passive margin*. Swiss J. Geosci., 110, 833-850, doi: 10.1007/s00015-017-0280-5.

Picotti S., Francese R., Giorgi M., Pettenati F. and Carcione J.M.; 2017: *Estimation of glacier thicknesses and basal properties using horizontal-to-vertical component spectral ratio (HVSR) technique from passive seismic data*. J. Glaciol., 63, 229-248, doi: 10.1017/jog.2016.135.

Riva M., Besio M., Masetti D., Roccati F., Sapigni M. and Semenza E.; 1990: *La geologia delle valli Vaiont e Gallina (Dolomiti orientali)*. Annali Univ. Ferrara, Sez. Scienze della Terra, 2, 55-76.

Rizzo E. and Giampaolo V.; 2019: *New deep electrical resistivity tomography in the High Agri Valley basin (Basilicata, southern Italy)*. Geomatics, Nat. Hazards and Risk, 10, 197-218, doi: 10.1080/19475705.2018.1520150.

Schmidt-Hatterberger C., Bergmann P., Labitzke T., Wagner F. and Rippe D.; 2016: *Permanent crosshole electrical resistivity tomography (ERT) as an established method for the long-term CO2 monitoring at the Ketzin pilot site*. Int. J. Greenhouse Gas control, 52, 432-448.

Tejero-Andrade A., Argote-Espino D.L., Cifuentes-Nava G., Hernàndez-Quintero E., Chàvez R.E. and Garcia-Serrano A.; 2018: *'Illuminating' the interior of Kukulkan's Pyramid, Chichèn Itzà, Mexico, by means of non-conventional ERT geophysical survey*. J. Archaeolog. Sci., 90, 1-11.

Troiano A., Isaia R., Di Giuseppe M.G., Tramparulo F.D.A. and Vitale S.; 2019: *Deep electrical resistivity tomography for a 3D picture of the most active sector of Campi Flegrei caldera*. Sci. Rep., 9, 15124, doi: 10.1038/s41598-019-51568-0.

Corresponding author: Roberto G. Francese
Università degli Studi di Parma
Department of Chemistry, Life and Environmental
Sustainability Sciences (S.C.V.S.A.)
Parco Area delle Scienze 157/A, 43124 Parma, Italy
Phone: +39 0521 905315, e-mail: roberto.francese@unipr.it